ANL/MSD/CP--84926

MRS Spring Mtg., San Francisco, CA, '95

CONF-950412--60

Magnetic Phase Transitions in Epitaxial Fe/Cr Superlattices‡

Eric E. Fullerton,* K.T. Riggs,*,+ C.H. Sowers,* A. Berger, and S.D. Bader***

**Materials Science Division*
Argonne National Laboratory, Argonne, IL 60439

***Department of Physics and Institute of Surface and Interface Science*
University of California-Irvine, Irvine, CA 92717

Proceedings of the 1995 Spring Meeting of the Materials Research Society, Vol. 384 "Magnetic Ultrathin Films, Multilayers and Surfaces", held April 17-21, 1995, San Francisco, CA

*Work supported by the U.S. Department of Energy, Basic Energy Sciences-Materials Sciences, under contract #W-31-109-ENG-38 (Argonne) and support from the Alexander von Humboldt-Stiftung through a Feodor Lynen Research Fellowship (AB).

+Permanent address: Stetson University, DeLand, FL 32720.

Magnetic Phase Transitions in Epitaxial Fe/Cr Superlattices‡

Eric E. Fullerton,* K. T. Riggs,*,+ C. H. Sowers,* A. Berger,** and S. D. Bader*

*Materials Science Division
Argonne National Laboratory, Argonne, IL 60439, USA

**Department of Physics and Institute of Surface and Interface Science,
University of California-Irvine, Irvine, CA 92717

Abstract

The surface spin-flop and Néel transitions are examined in Fe/Cr superlattices. The surface spin-flop, originally predicted by Mills [Phys. Rev. Lett. **20**, 18 (1968)], is observed in Fe/Cr(211) superlattices with antiferromagnetic interlayer coupling and uniaxial in-plane anisotropy. The Néel transition (T_N) of Cr is observed in Fe/Cr(001) superlattices, for which the onset of antiferromagnetism is at a thickness t_{Cr} of 42Å. The bulk value of T_N is approached asymptotically as t_{Cr} increases and is characterized by a three-dimensional shift exponent. These T_N results are attributed to finite-size effects and spin-frustration near rough Fe-Cr interfaces.

Introduction

Fe/Cr superlattices exhibit the intriguing magnetic properties of oscillatory interlayer coupling [1,2] and giant magnetoresistance [3]. Growth of epitaxial Fe/Cr superlattices allows the interlayer coupling and magnetic anisotropy to be tailored in order to probe additional, rather subtle, magnetic transitions. We discuss two such transitions, the surface spin-flop transition in Fe/Cr(211) superlattices [4] and the Néel transition of thin Cr layers in proximity with Fe in Fe/Cr(001) superlattices. The surface spin-flop transition is a first-order, field-induced phase transition in antiferromagnets with uniaxial magnetic anisotropy and the magnetic field applied along the easy axis. It was first predicted over 25 years ago, [5] but not realized experimentally until the appearance of Ref. 4. In Fe/Cr(100) superlattices, the antiferromagnetic ordering of the Cr spacers results in anomalies in a variety of physical properties. The Néel temperature (T_N) is strongly dependent on the Cr thickness. A transition-temperature shift exponent is extracted from the data in the thick Cr regime (<160Å) and discussed in terms of a combination of finite-size effects and spin-frustration near rough Fe/Cr interfaces. Results are compared with mean-field calculations of a two-dimensional Ising system at finite temperature to get rudimentary insight into the problem. The work provides auxiliary demonstrations of the value of epitaxial superlattices grown via sputtering, and of the versatility of a recent magneto-optic simulation formalism to handle different and arbitrary magnetization orientations in each ferromagnetic layer within a multilayer structure.

Fe/Cr(100) and (211) superlattices were epitaxially grown by d.c. magnetron sputtering onto single-crystal MgO(100) and (110) substrates, respectively. The epitaxial relations are Fe/Cr[011] // MgO[001] for Fe/Cr(100) and Fe/Cr[ ] // MgO[001] for Fe/Cr(211). The growth procedure and structural characterizations are provided elsewhere [6]. The magnetic properties were measured by means of a SQUID magnetometer and the surface magneto-optic Kerr effect using p-polarized, 633-nm light. Transport properties were measured using a standard four-terminal d.c. technique with a constant current of 10 mA and the applied field H in-plane.

Surface spin-flop transition

In a MnF_2-type antiferromagnet (AF), a magnetic field parallel to the easy axis induces a first-order phase transition from the spin sublattices being antiparallel along the easy axis direction to the spin-flop phase in which the spin sublattices reorient almost 90° from the field direction but canted toward it. The spin-flop transition occurs at a field H_{SF} given by

$$H_{SF} = \sqrt{2H_E H_A + H_A^2} \quad , \qquad (1)$$

where H_E and H_A are the exchange and anisotropy fields, respectively. For a thin AF film, surface effects strongly influence the magnetic response of the system [4,5,7,8]. The lower coordination of the surface spins allow them to respond more easily to external fields. If the surface spin is pointed antiparallel to the external field, the surface is expected to undergo a surface spin-flop transition at a lower field of $\approx H_{SF}/\sqrt{2}$.

Experimental searches of the MnF_2 system for the surface spin-flop transition at the time of the original theoretical prediction were unsuccessful. In the work of Ref. 4 Fe/Cr(211) superlattices were utilized. In these structures, the spin configuration is predominantly governed by: (i) the Zeeman interaction of the Fe with the external field, (ii) the AF interlayer coupling across the Cr spacers, and (iii) a uniaxial, in-plane anisotropy for the Fe. Therefore, these superlattices are isomorphic to the MnF_2-class antiferromagnets with a (100) surface.

Consider a superlattice which contains N layers of Fe. If N is even, then the two terminal Fe layers will point antiparallel to each other. Therefore, in an applied field, one of the surface layers will be antiparallel to the external field and will undergo the surface spin-flop transition. If N is odd, then the two terminal Fe layers will be parallel and align with the field, and only a bulk spin-flop transition is observed. Figure 1 shows both theoretical [4] and experimental results for superlattices with an even number of magnetic layers.

Shown in Fig. 1a is the calculated magnetization curve as a function of applied field for an N=16 superlattice with HA=0.5 kOe and HE=2.0 kOe. For small values of H, the Fe layers are

antiparallel and aligned along the easy axis. As H increases the system undergoes a surface spin-flop transition at 0.93 kOe which is less than the expected spin-flop field of 1.5 kOe predicted from Eq. (1). For higher fields, the surface spin-flop transition evolves in a quasi-continuous manner into the bulk spin-flop transition, as originally predicted by Keffer and Chow [9] and described in detail in Refs. 4 and 7.

Shown in Fig. 1b are the magnetization curves for a (211)-oriented [Fe(40 Å)/Cr(11 Å)]N=22 superlattice. The magnetization curves were measured using SQUID magnetometry and Kerr effect from H = -4 kOe to +4 kOe with H along the easy axis. As was observed in the theoretical calculations, the system undergoes two transitions upon going from the plateau at low fields into the canted state at higher fields. These two transitions can be seen more vividly in Fig. 1c which shows a static susceptibility plot obtained from differentiating the magnetization data. Two peaks are observed and identified in the figure as S and B for the surface and bulk spin-flop transitions, respectively. Similar measurements on superlattices with an odd number of layers show only the bulk transition as expected.

To confirm that the transition at the lower field results from the surface, we compare the SQUID results with Kerr-effect measurements. The Kerr-effect is surface sensitive, by virtue of the optical skin depth, which should reflect itself as a stronger intensity for the surface transition. In the Kerr intensity measurements (Fig. 1b) for H<0, the bulk spin-flop transition is reduced and the surface spin-flop transition is enhanced relative to their strengths of the SQUID magnetization measurements. At the surface spin-flop transition, the Kerr intensity switches from negative to positive, which indicates that the top Fe layer is oriented in opposition to H for small negative fields. As H crosses over to positive fields, the top Fe layer is aligned with the field; the surface spin-flop initiates from the Fe layer closest to the substrate, and is not observed by Kerr and only seen in the SQUID results.

To compare the Kerr results with the theoretical model, we have calculated the expected Kerr response for the model superlattice (dashed line in Fig. 1a) using the formalism of Zak et al. [10]. The formalism has the versatility to generate the magneto-optic response of a multilayer

system where each of the N magnetic layers has arbitrary angles with respect to . The calculated Kerr response exhibits all the qualitative features of the measured spectrum. In the canted region of H>HSF, the Kerr signal is higher than the SQUID magnetization which results from the surface layers being canted closer to than the bulk layers. Quantitative differences between the calculated and measured response arise from the different number of magnetic layers and the additional experimental contributions of cubic anisotropies and biquadratic coupling which are not included in the model Hamiltonian.

Shown in Fig. 2 is a second example of the surface transition in a (211)-oriented [Fe(14 Å)/Cr(11 Å)]44 superlattice. The large number of layers makes the surface transition very difficult to resolve in the SQUID measurement. However, the Kerr measurement dramatically enhances the surface transition with respect to the bulk transition. In contrast to the previous example, the Kerr results are symmetric about the origin indicating that the surface transition is equally likely to initiate from the substrate or top surface.

This study provided the first experimental observation of the surface spin-flop transition. The surface contributions to the magnetic response of the superlattice is elucidated by the combination of SQUID which measures the total magnetization and Kerr effect which is sensitive to the vicinity of the illuminated surface. This example highlights the rich magnetic phases possible in coupled magnetic superlattices.

Cr Néel transition

An outstanding problem in understanding the interlayer coupling in Fe/Cr superlattices is the role of the magnetic ordering within the Cr spacers. Bulk Cr is an itinerant AF with $T_N = 311$ K. An incommensurate spin-density wave (SDW) is formed which is characterized by a wave vector Q determined by the nested feature in the <100> direction of the Cr Fermi surface. At high temperature, the Cr spin sublattices S are transverse to Q ($S \perp Q$), while below the spin-flip transition at 123K S rotates 90° to form a longitudinal SDW with $S \| Q$ [11].

For the case of Cr(100) spacers, two periods in the interlayer coupling have been observed, a short period [two monolayers (ML)] and a long period (18Å) [2,12-14]. The short-period oscillations results from the same nesting responsible for the SDW of bulk Cr. The long period has also been observed in (110) [2] and (211) [6] oriented films, which suggests that it is not related to the nesting but, results instead from a short spanning-vector associated with the relatively isotropic 'lens' feature of the Fermi surface [15]. In general, only the long-period oscillation is observed in superlattices. Atomic steps in the Fe-Cr interface are sufficient to suppress the short period coupling. However, the magnetic ordering of the Cr in the presence of a stepped or rough interface and its role on the interlayer coupling are not known. Slonczewski [16,17] predicted that fluctuations in the short-period interactions can give an additional non-oscillatory, biquadratic coupling term in which the magnetization orientation between adjacent Fe layers is 90°, rather than 180° or 0°. This extrinsic biquadratic coupling can become a prominent characteristic of the thick Cr-spacer regime in which the long-period coupling is weak.

In the present work, the AF ordering of Cr spacer layers in sputtered, epitaxial Fe/Cr(001) superlattices is considered and we report a number of new observations. Firstly, we find that the AF order is suppressed for Cr spacers of thickness t_{Cr}<42Å. Secondly, for t_{Cr}>42Å, T_N initially rises rapidly, asymptotically approaches the bulk value for the thickest spacers studied (165Å), and exhibits a transition-temperature shift exponent λ=1.4±0.3 characteristic of three-dimensional (3D) Heisenberg or Ising models. The overall T_N-vs.-t_{Cr} behavior can be understood in terms of a combination of finite-size and spin-frustration effects. Thirdly, the AF ordering of the Cr spacers results in anomalies in a variety of physical properties, including the interlayer coupling, remanent magnetization (M_r), coercivity (H_c), resistivity (ρ) and magnetoresistance (MR). Finally, the biquadratic coupling of the Fe layers observed for $T>T_N$ vanishes below T_N.

Transport measurements are often used as a probe of the AF ordering in Cr and Cr alloys, where ρ is enhanced above its extrapolated value as the temperature T decreases through T_N [11,18]. This anomaly in r, attributed to the formation of energy gaps opening on the nesting parts of the Fermi surface, is commonly used to locate T_N. Shown in Fig. 3 are T-dependent transport

results for an [Fe(14Å)/Cr(70Å)]13 superlattice. Figure 3(a) shows ρ vs. T for H=500 Oe, which is a sufficient field to align the Fe magnetization. An anomaly in ρ below ~200K is observed as an increase above its expected linear behavior, as shown by the dotted line. The difference between the measured r and the linear extrapolation rlin is plotted in Fig. 3(b). The 7% enhancement in ρ at 190K is consistent with similar measurements in bulk Cr and Cr(001) films [11,19]. The reduced value of T_N=195 K is determined by the point of inflection of ρ vs. T [see Fig. 3(c)].

The AF-ordering of the Cr dramatically alters the magnetic properties of the superlattices. Shown in Fig. 4 is the T dependence of M_r, H_c, the saturation field (H_s), and the MR of the same superlattice as in Fig. 3. All four of these quantities exhibit anomalous behavior which is directly related to the Néel transition of the Cr. The M_r shows a transition at T_N from a value of 0.53Ms for $T>T_N$ to $\approx 0.95M_s$ for $T<T_N$. The Hc value peaks at T_N in a manner often observed in systems which undergo magnetic phase transitions [20]. H_s in Fig. 3(c), the field at which M reaches 90% of M_s, is roughly proportional to the interlayer coupling strength, and increases strongly with decreasing $T>T_N$, reaches a maximum at ~230K, and then decreases sharply and approaches zero at T_N. The MR in Fig. 4(d) also shows an anomaly at T_N, and its decrease is consistent with a loss of interlayer coupling below T_N. The M_r value for $T>T_N$ is consistent with a 90° alignment of the magnetization of adjacent Fe layers, indicative of biquadratic interlayer magnetic coupling, while the Mr value for $T<T_N$ is consistent with a vanishing of the biquadratic coupling that leaves the layers relatively uncoupled. This conclusion has been confirmed by neutron reflectivity on a similar superlattice which indicates 90° alignment of adjacent Fe layers for $T>T_N$ [21].

Utilizing both the transport and magnetic properties to identify T_N, Fig. 5 shows T_N vs. t_{Cr} for a series of (001)-oriented Fe(14Å)/Cr(t_{Cr}) superlattices. For $t_{Cr}<42$Å there is no evidence of the Cr ordering. For $t_{Cr}>42$Å T_N increases rapidly and reaches a value of 265K for a 165-Å Cr thickness. For a 3000-Å thick Cr film grown in similar fashion to the superlattices, a T_N value of 295K was obtained. A number of factors can alter the T_N value of Cr, including impurities, strains and defects [11,19]. Studies of Cr(001) films on LiF(001) substrates reported thickness dependent T_N values attributed to epitaxial strain [19]. The behavior of T_N vs. t_{Cr} reported herein can be

understood as arising from a combination of finite-size effects within the Cr spacer and spin-frustration effects at the Fe-Cr interface, as is discussed in what follows.

In thin films, magnetic properties are altered due to the surface contribution to the free energy [22]. Since this contribution is generally positive, the magnetic order is weakened at the surface and the ordering temperature is reduced. Scaling theory predicts that T_N should have the form:

$$\frac{T_N(\infty) - T_N(t_{Cr})}{T_N(t_{Cr})} = b\, t_{Cr}^{-\lambda} \quad , \qquad (2)$$

where $\lambda=1/\nu$ is the shift exponent, b is a constant and ν is the correlation-length exponent for the bulk system. The theoretically expected λ values are 1/0.7048=1.419 [23] and 1/0.6294 = 1.5884 [24] for the 3D Heisenberg and Ising models, respectively. Fitting the data for t_{Cr}>70Å to Eq. (2) is shown by the dashed line in Fig. 5, where $T_N(\infty)$=295K has its thick-film value. These data are well represented by $\lambda\approx1.4\pm0.3$, which is in agreement with expectation from scaling theory. To fit the complete data set, we use the empirical expression:

$$\frac{T_N(\infty) - T_N(t_{Cr})}{T_N(t_{Cr})} = b\,(t_{Cr} - t_0)^{-\lambda'} \quad , \qquad (3)$$

where t_0= 42.3Å represents the zero offset in the Cr thickness and $\lambda'=0.8\pm0.1$ as shown by the solid line in Fig. 5. The sharp drop in the value of T_N near t_{Cr}~50Å and the nonuniversal value of λ' indicates the presence of an additional effect for the thinnest Cr spacers that we will identify below as being due to spin frustration.

For an ideal Fe/Cr(001) interface, $T_N(t_{Cr})$ should increase with decreasing Cr thickness due to the Fe-Cr exchange coupling since the Fe Curie temperature is much higher than T_N for Cr. This agrees with the experimental observations of Ref. 25 that the surface-terminated ferromagnetic layer of Cr on an Fe(001) substrate oscillates in its magnetization orientation relative to that of the Fe with a ≈2-ML period, consistent with the SDW AF anticipated for Cr. The oscillations are observed well above the bulk T_N, which suggests that the substrate, a relatively

perfect Fe whisker, stabilizes the AF spin structure of the Cr. In the present study, however, we find $T_N(t_{Cr})$ decreases for thin Cr layers. We believe that this behavior arises from spin-frustration effects in the vicinity of the rough Fe-Cr interfaces. Such interfaces contain atomic steps as shown in the Fig. 5 inset. The interfacial exchange energy can be minimized only locally, and frustration of the interfacial spins will occur if the Fe and Cr magnetically order long-range. In the Fig. 5 inset, excess magnetic energy is schematically located at the Fe-Cr interface to the right of the step where the Fe and Cr moments are forced to align ferromagnetically. For a superlattice, assuming random monatomic steps at both the Fe and Cr surfaces, 25% of the Cr layer will be frustrated at both interfaces, 50% will be frustrated at one interface, and 25% will match with the Fe layers. The value of T_N, therefore, should be influenced by a balance between the energy gained from long-range AF ordering of the Cr and the energy cost due to magnetic frustration at the Fe-Cr interfaces. For thin Cr layers, the frustration energy is sufficiently high to suppress long-range ordering of the Cr. As t_{Cr} increases, the system overcomes the frustration energy and begins to order. The crossover thickness for the present samples is 42Å of Cr.

To further understand the mechanism for suppressing the Cr ordering, we have performed mean-field calculations at finite temperatures for an AF layer sandwiched between two ferromagnetic (F) layers as shown in Fig. 6. The model utilizes periodic boundary conditions, and the F, interface and AF exchange coupling constants are given by JF= -1.88JI = -3.35JAF. The ferromagnetic layers are given by the open squares and the AF layer is represented by the circles. The circle are gray-scaled to represent the moment of the layer. Each ferromagnetic layer has two atomic steps to induce spin-frustration in the system.

Two stable magnetic configurations are identifies in the calculations and shown in Fig. 6. The striped regions in the AF layer represent walls which separate AF domains which are 180° out of phase. In one configuration (upper panel), the domain walls go across the AF layer connecting steps on adjacent ferromagnetic layers. In the other stable configuration (lower panel) the domain walls are parallel to the interface and connect steps on the same ferromagnetic layer. In this configuration, the center of the AF layer exhibits homogeneous long-range order. For thin AF

layers, the upper configuration is the lowest energy configuration. For thicker layers, the lower panel represents the lowest energy configuration. For this model structure, a crossover at 18 ML is shown in the phase diagram of Fig. 7. Below 18 ML layer thicknesses the upper-panel configuration is lowest energy for all temperatures. Above 18 ML, the lower panel is lowest energy and T_N approaches T_N for a free standing film for increasing AF layer thicknesses.

Although this model is too simplistic to quantitatively describe the Fe/Cr system, it is able to reproduce salient qualitative features of our measurements and highlights the important role roughness plays in the magnetic ordering of the Fe/Cr(001) system. More realistic electronic structure calculations [26] of Fe/Cr/Fe trilayers determine that the energy cost in suppressing the Cr moment (at 0 K) is only 0.8 meV/atom, as compared to 200 and 80 meV/atom for Fe and Mn, respectively. Theoretical calculations of diffuse or stepped Fe/Cr interfaces demonstrate that the presence of frustrated Fe-Cr bonds can strongly suppress the Cr moment over extended distances [26-28]. Thus, Cr is highly sensitive to its local environment with local distortions being capable of causing strong moment reductions. This again supports the idea that roughness plays a dominant role in the magnetic ordering.

In summary, we have investigated the AF-ordering of Cr spacer layers in epitaxial Fe/Cr(001) superlattices. AF order is suppressed for Cr spacers of thickness t_{Cr}<42Å and is attributed to spin-frustration effects. For t_{Cr}>42Å T_N initially rises rapidly, and then asymptotically approaches the bulk value for the thickest spacers studied (165Å) with a transition-temperature shift exponent characteristic of 3D Heisenberg or Ising models. Finally, the AF ordering of the Cr spacer layers dramatically alters the interlayer coupling in the sense that the biquadratic coupling of the Fe layers observed for $T>T_N$ vanishes below T_N.

We thank J. Mattson, D. Stoeffler, R. Wang and D. Mills for helpful discussion and R. Wang and D. Mills for supplying the spin-configurations of their model calculations. Work supported by the U.S. Department of Energy, Basic Energy Sciences-Materials Sciences, under contract #W-31-109-ENG-38. One of us (A.B.) gratefully acknowledges support from the Alexander von Humboldt-Stiftung through a Feodor Lynen Research Fellowship.

References

† Permanent address: Stetson University, DeLand, FL 32720.

1. P. Grünberg, R. Schreiber, Y. Pang, M. B. Brodsky, and C. H. Sowers, Phys. Rev. Lett. **57**, 2442 (1986).
2. S. S. P. Parkin, N. More, and K. P. Roche, Phys. Rev. Lett. **64**, 2304 (1990).
3. M. N. Baibich, J. M. Broto, A. Fert, F. N. VanDau, F. Petroff, P. Etienne, G. Creuzet, A. Friederich, and J. Chazelas, Phys. Rev. Lett. **61**, 2472 (1988).
4. R. W. Wang, D. L. Mills, E. E. Fullerton, J. E. Mattson, and S. D. Bader, Phys. Rev. Lett. **72**, 920 (1994).
5. D. L. Mills, Phys. Rev. Lett. **20**, 18 (1968).
6. E. E. Fullerton, M. J. Conover, J. E. Mattson, C. H. Sowers, and S. D. Bader, Phys. Rev. B **48**, 15755 (1993).
7. R. W. Wang and D. L. Mills, Phys. Rev. B (1994).
8. A. S. Carrico, R. E. Camley, and R. L. Stamps, Phys. Rev. B **50**, 13453 (1994).
9. F. Keffer and H. Chow, Phys. Rev. Lett. **31**, 1061 (1973).
10. J. Zak, E. R. Moog, C. Liu, and S. D. Bader, Phys. Rev. B **43**, 6423 (1991).
11. E. Fawcett, Reviews of Modern Physics **60**, 209 (1988).
12. J. Unguris, R. J. Celotta, and D. T. Pierce, Phys. Rev. Lett. **67**, 140 (1991).
13. D. T. Pierce, J. A. Stroscio, J. Unguris, and R. J. Celotta, Phys. Rev. B **49**, 14564 (1994).
14. S. T. Purcell, W. Folkerts, M. T. Johnson, N. W. E. McGee, K. Jager, J. ann de Stegge, W. B. Seper, W. Hoving, and P. Grünberg, Phys. Rev. Lett. **67**, 903 (1991).
15. D. D. Koelling, Phys. Rev. B **50**, 273 (1994).
16. J. C. Slonczewski, Phys. Rev. Lett. **67**, 3172 (1991).
17. J. C. Slonczewski, J. Magn. Magn. Mater. (in press).
18. E. Fawcett, H. L. Alberts, V. Y. Galkin, D. R. Noakes, and J. V. Yakhmi, Reviews of Modern Physics **66**, 25 (1994).
19. J. Mattson, B. Brumitt, M. B. Brodsky, and J. B. Ketterson, J. Appl. Phys. **67**, 4889 (1990).

20. S. D. Bader, D. Li, and Z. Q. Qiu, J. Appl. Phys. **76**, 6419 (1994).

21. S. Adenwalla, G. P. Felcher, E. E. Fullerton, and S. D. Bader, unpublished.

22. K. Binder, in Phase Transitions and Critical Phenomena, edited by C. Domb & J. L. Lebowitz (Academic Press, London, 1983), p. 1.

23. K. Chen, A. M. Ferrenberg, and D. P. Landau, Phys. Rev. B **48**, 3249 (1993).

24. A. M. Ferrenberg and D. P. Landau, Phys. Rev. B **44**, 5081 (1991).

25. J. Unguris, R. J. Celotta, and D. T. Pierce, Phys. Rev. Lett. **69**, 1125 (1992).

26. D. Stoeffler and F. Gautier in Magnetism and Structure in Systems of Reduced Dimension, edited by B. Dieny R. F. C. Farrow M. Donath, A. Fert, B. D. Hermsmeier (Plenum Press, New York, 1993), p. 411.

27. D. Stoeffler and F. Gautier, Phys. Rev. B **44**, 10389 (1991).

28. D. Stoeffler and F. Gautier, J. Magn. Magn. Mat. (submitted).

Figure Captions

Figure 1: (a) Magnetization results for a model 16-layer superlattice structure. The solid line is the magnetization and the dashed line is the calculated longitudinal magneto-optic Kerr effect. (b) Magnetization curve of a [Fe(40 Å)/Cr(11 Å)]22 superlattices from -Ms to Ms with the applied field parallel to the magnetic easy axis. The solid line is measured by a SQUID magnetometer and the dashed line is measured by longitudinal magneto-optic Kerr effect. (c) The numerical derivative of the measured curves in (b). S and B refer to the surface and bulk spin-flop transitions, respectively.

Figure 2: Magnetization curves of a (211)-oriented [Fe(14 Å)/Cr(11 Å)]44 superlattice with H parallel to the magnetic easy axis. The solid line is by SQUID magnetometry and the dashed line is Kerr effect. The surface and bulk spin-flop transitions are indicated by S and B, respectively.

Figure 3: Resistivity of an [Fe(14Å)/Cr(70Å)]13 superlattice. (a) r vs. T measured at H=500 Oe. The dashed line is a linear extrapolation of the data above 280 K. (b) The difference between the measured ρ and the linear extrapolation rlin normalized to rlin. (c) Derivative of ρ smoothed for clarity. The minimum in dρ/dT locates T_N.

Figure 4: Temperature dependent magnetization results for the superlattice shown in Fig. 3. (a) Squareness ratio M_r/M_s; (b) coercivity, (c) saturation field defined at 90% of M_s, and (d) the magnetoresistance. The vertical dashed line locates T_N of the Cr interlayers.

Figure 5: T_N for a series of [Fe(14Å)/Cr(t_{Cr})]N superlattices vs. Cr thickness. The dashed and solid lines are fits to Eq. (2) and (3), respectively. The inset shows a possible spin configuration of Cr on a stepped Fe surface in which the region of spin frustration at the Fe-Cr interface is shown schematically by the shaded ellipse to the right of the atomic step rature mean-field calculations of a F/AF/F trilayer structure. The circles and open squares.

Figure 6: Finite-temperatures are the AF and F layers, respectively. The circles are gray-scaled to represent the moment; filled and open correspond to full and zero moment, respectively.

Figure 7: Néel temperatures for AF-layer (solid circles) calculated for the model shown in Fig. 6 versus AF layer thickness. The solid line is a similar calculation for a free standing AF film.

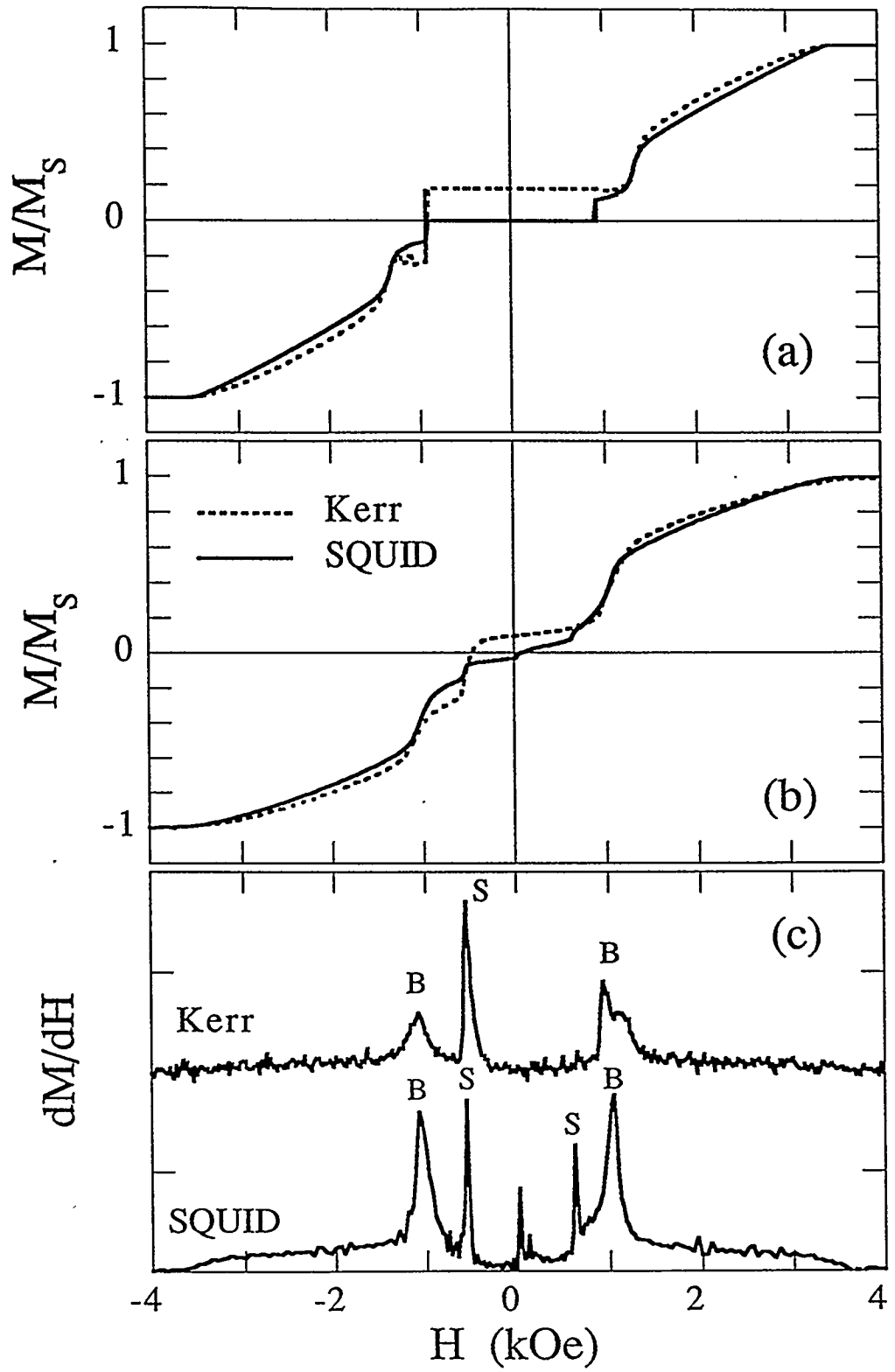

Fig. 1

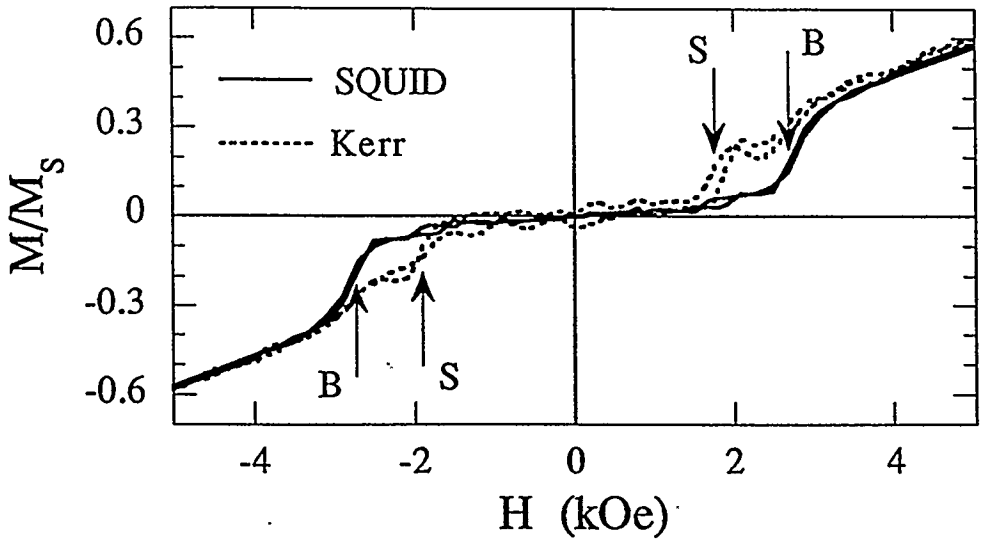

Fig. 2

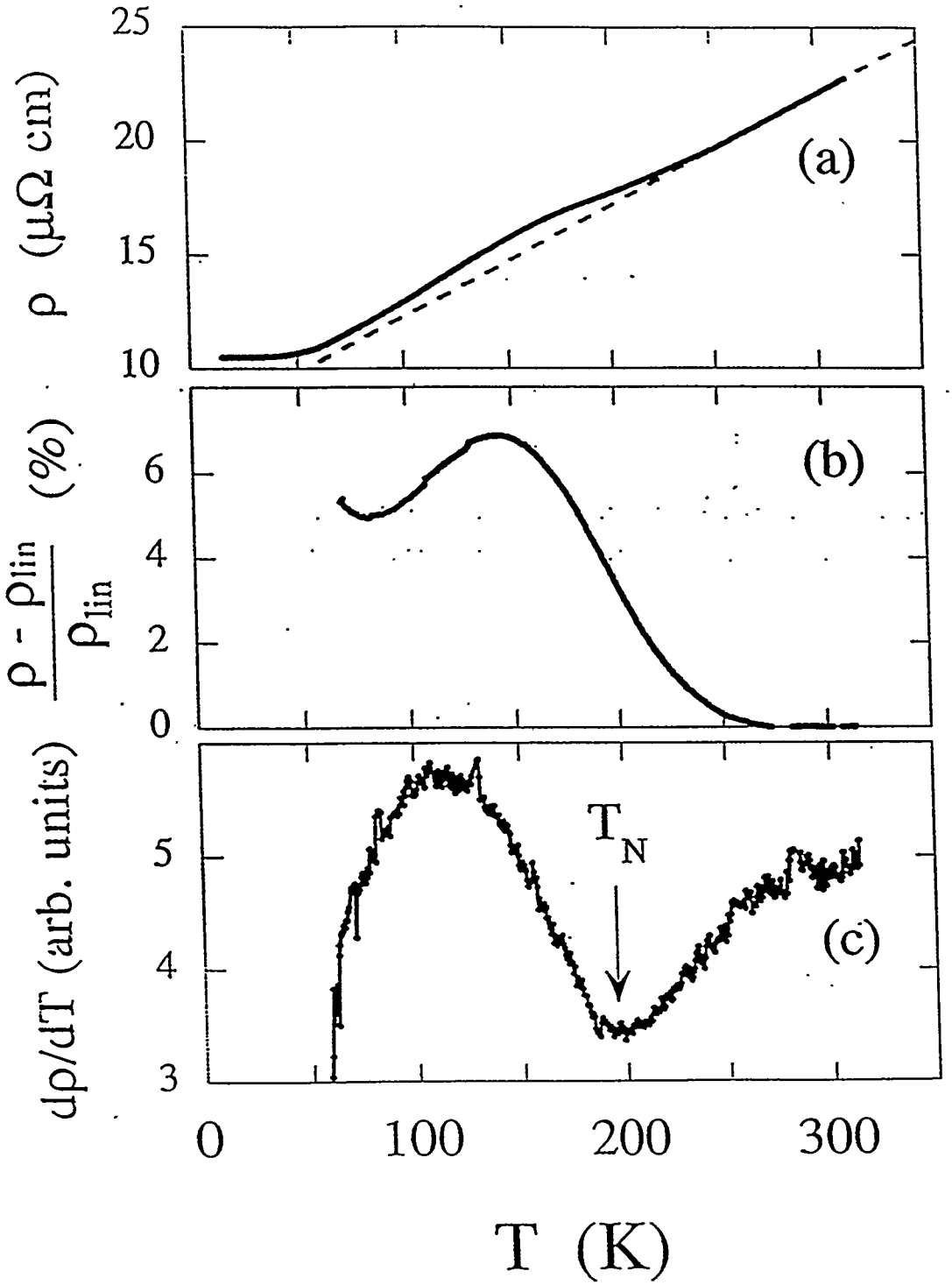

Fig. 3

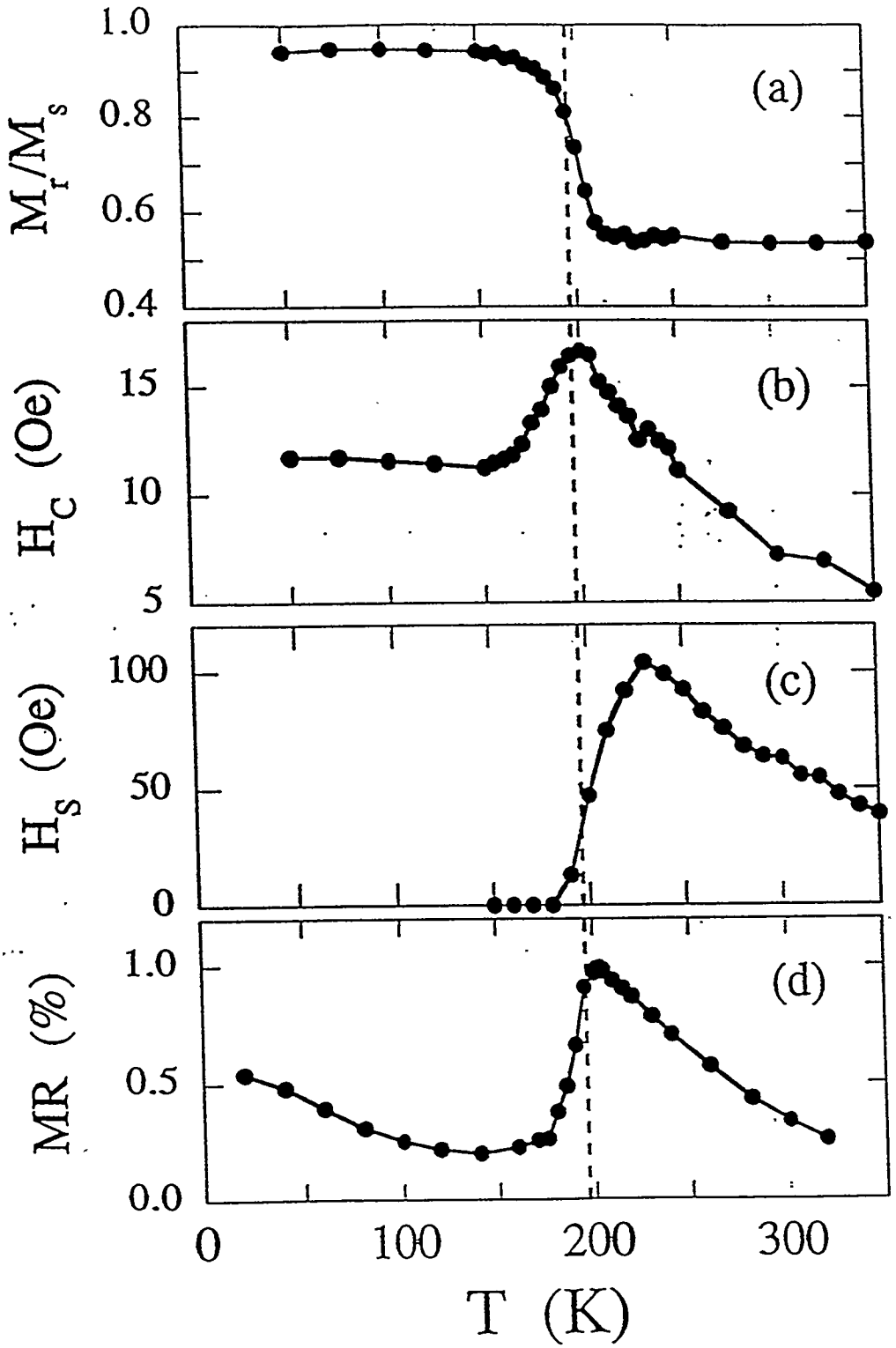
1.0
0.8
0.6
0.4
M_r/M_s
(a)
15
10
5
H_C (Oe)
(b)
100
50
0
H_S (Oe)
(c)
1.0
0.5
0.0
MR (%)
(d)
0
100
200
300
T (K)

Fig. 4

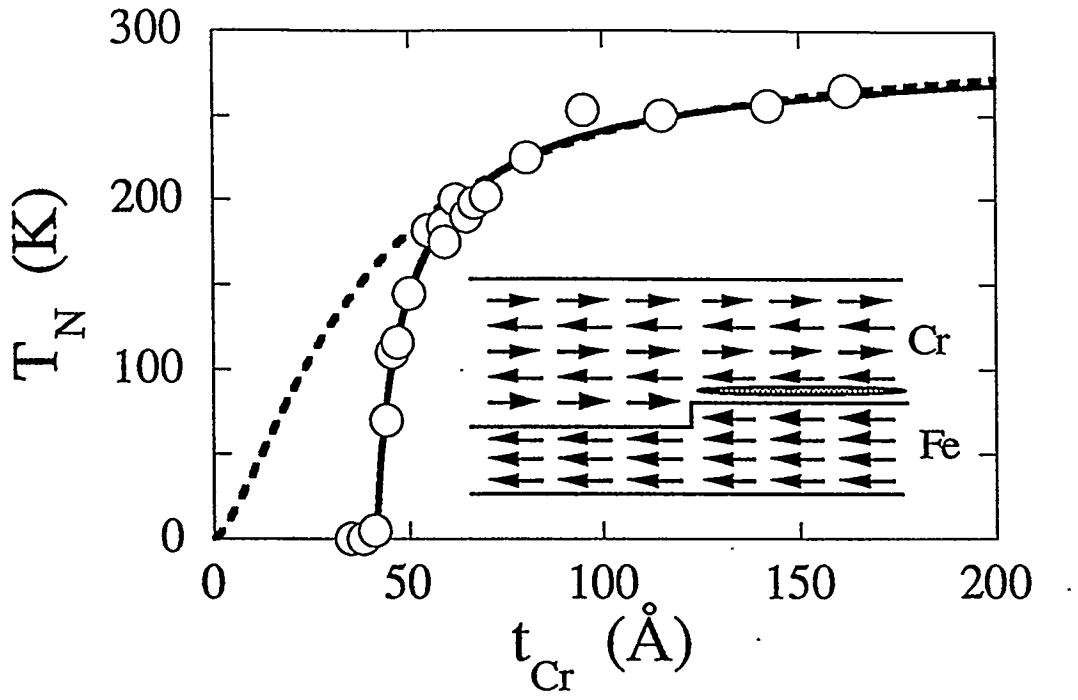

Fig. 5

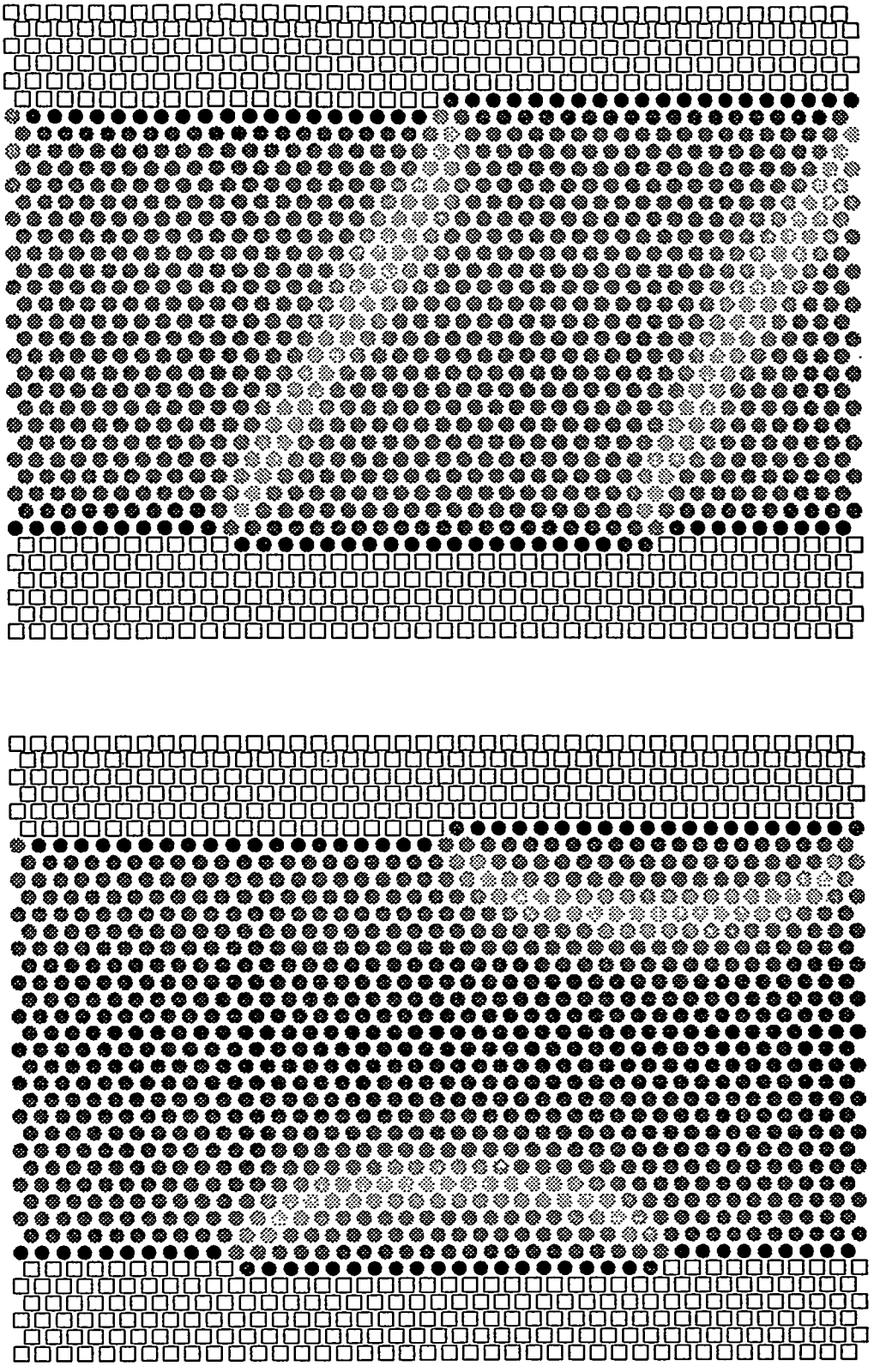

Fig. 6

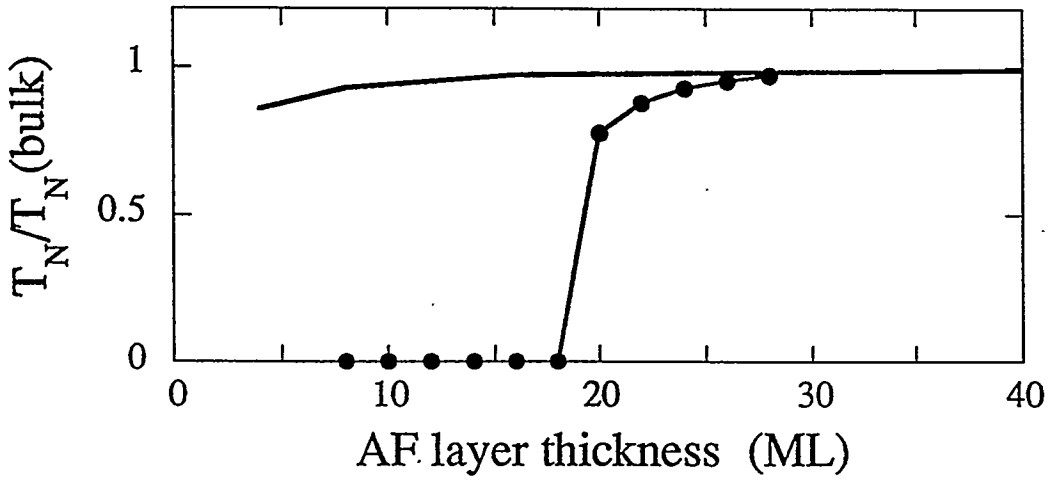

Fig. 7